Journal of New Materials for Electrochemical Systems 19, 121-130 (2016)

Pd Octahedral and Spherical Nanocrystals Supported on Crumpled Graphene Oxide: Their Comparative Studies for Electrocatalytic Applications

Majid Khan[1,*], Ammar Bin Yousaf[2,†] and Muhammad Imran[2]

[1]Department of Physics, Abdul Wali Khan University, Mardan 23200, Pakistan
[2]Hefei National Laboratory for Physical Sciences at Microscale, Department of Nano Chemistry,
School of Chemistry and Material Science, University of Science and Technology of China, Hefei 230026, China

Received: April 11, 2016, Accepted: July 10, 2016, Available online: August 30, 2016

Abstract: *Palladium (Pd) octahedral and spherical nanocrystals (NCs) were successfully synthesized on crumpled graphene oxide (GO) by surface adsorption of H_2 and CO in the presence of capping agent poly(vinylypyrrolidone) (PVP). Their comparative studies as anode material for direct methanol fuel cells (DMFCs) have been measured by hydrogen evolution reaction (HER) performance and methanol oxidation reaction (MOR) activity. The electrocatalytic properties of both the nanocrystals were studied in $HClO_4$ acidic media and compared with each other. Pd octahedral nanocrystals have shown the best performance as an anode material, their onset potential for evolution of hydrogen from the active sites of the catalyst is more towards zero than the spherical NCs. The observed specific activity (ca. 4.3 $mA.cm^{-2}$) and mass activity (ca. 5300 $mA.mg^{-1}$) of Pd towards MOR is much higher for octahedral NCs than that of spherical NCs.*

Keywords: Pd nanocrystals; Graphene oxide; Surface adsorption; Hydrogen evolution reaction; Methanol oxidation reaction

1. INTRODUCTION

Noble metal nanocrystals have attracted much research attention for their use in photonics, sensing, thermal, and magnetic as well as catalytic properties [1-4]. Their physical and chemical properties can easily be tuned by controlling the size and shape. Size determines the ratio of surface to bulk atoms specifically, and surface area. Shape controls the facets and thus the surface structure of a nanocrystal, as well as the fractions of atoms at corners and edges. Moreover, shape has more importance than the size and other parameters and it offers greater versatility in tunning the catalytic properties of a nanocrystal, especially when the atoms at different facets possess different activities [5]. Although, for face-centered cubic (fcc) metals, the morphology and surface of their nanocrystals are closely related subjects of matter, however, their properties depend differently upon the morphology and surface structure of the nanocrystals [6-7]. For example, as a surface property, catalysis of noble metal nanocrystals are concerned more of their surface structure [8-9]. Previously, a number of different synthetic strategies have been developed to control the morphology of noble metal nanocrystals [10]. Up to date, solution-based methods have developed as a versatile approach for controlled synthesis of noble metal nanocrystals and their alloys, where it is important to generate zero-valent noble metal through reduction of the metal ions in the presence of stabilizing agents. For Pd, many different shapes have been accomplished by controlling the thermodynamics or kinetics involved in nanocrystal growth. When the growth is under thermodynamic control, the product will have the lowest surface energy. In this case, the capping agent plays an important role in shaping the final product's by changing the order of surface energies for different facets through selective adsorption and thus their growth rates [11]. Where, the product of a kinetically controlled synthesis can significantly deviate from the thermodynamically favored structure that includes high index facets or concave surfaces [12].

For Pd and Pt nanocrystals, recently, the surface adsorption method has also been established in which strong and specific surface adsorption of small adsorbates as reducing agents have appeared as a dominant approach to control the surface structure of their nanocrystals [13-14]. Specific adsorption of small adsorbates controls only the surface structure of Pd and Pt nanocrystals, other factors further than the specific adsorption have been employed to improve the morphology of noble metal nanocrystals. A wide range of reducing agents have been used to prepare noble metal

To whom correspondence should be addressed:
*Email: majidkhan@awkum.edu.pk, majids@hotmail.com
*,† These authors contributed equally to this work

nanoparticles, including hydrogen, carbon monoxide, metal hydrides, hydrazine, hydroxyl amine, ascorbic acid, citric acid and vitamin B [15]. Hydrogen in particular is an effective reducing agent for noble metal salts in aqueous or non-aqueous solutions. Importantly, it provides a clean, reducing atmosphere with no harmful byproducts produced during the reactions [16]. Furthermore, the use of hydrogen decouples the effect of the reducing agent and stabilizing agent on the nucleation and any preferential directional growth of the particles. Recently, hydrogen has been used in aqueous media as a reducing agent in decorating different 2D nanostructures with Pd, Pt and Ru nanoparticles [17]. CO has also been employed as a powerful reducing and shaping agent in the last decade. It's adsorption properties have been determined on different surfaces of metal nanocrystals. In case of Pt, co-adsorption of CO and amines makes Pt{100} more energetically stable than Pt{111} and thus prompts the formation of Pt nanocubes [18-19]. CO favors to adsorb on Pd{111} surface and enables the growth of ultrathin Pd nanosheets having {111} as the main exposure surface and exhibiting catalytic properties as well as unique optical properties [20-21]. Two recent examples are, (1) the preferential growth of micrometer-long five-fold twinned Pd nanowires over Pd nanocubes under slow reduction and (2) the production of corolla-like Pd mesocrystals in the co-presence of Fe^{3+} as the oxidative etchant and CO as the surface controller [22]. In these two examples, the control over the surface adsorption by reduction kinetics and introducing oxidative etching to disturb the growth of seeds enrich the morphology of noble metal nanocrystals. Gang Fu et al., demonstrated that, CO specifically adsorbs on Pd (111), the adsorption strength and coverage of CO on Pd can be essentially varied by introducing H_2 to facilitate the formation of single-crystalline Pd tetrapod and tetrahedral nanocrystals enclosed by (111) surfaces. They have found that in the co-presence of CO and H_2 prepared tetrapod and tetrahedral nanocrystals. Upon aging in air, the as-prepared nanocrystals released hydrogen and were converted gradually to Pd nanocrystals. They have calculated conclusion by density functional theory (DFT) calculations, the formation of palladium hydride in the presence of H_2 weakens the chemisorption of CO and therefore helps to lower the CO coverage to induce the formation of Pd tetrapod nanocrystals [23].

In this work, we have evaluated the surface adsorption behavior of CO and H_2 by their reduction kinetics separately in the presence of same capping agent PVP to synthesize Pd octahedral and spherical NCs. Their catalytic activity as anode materials for DMFCs have been measured comparatively. Two types of results have been evaluated here, first basic electrocatalytic characterization analysis such as HER performance to remove the adsorbed hydrogen on the active sites of catalyst surface and second the MOR activity. The electrocatalytic activity for HER and MOR analysis give interesting results with a shape difference of the two same facets. MOR activity is presented here with respect to both the scales such as specific activity and mass activity.

2. EXPERIMENTAL SECTION

2.1. Chemicals and Materials

H_2PdCl_4 (99.9 % metal basis) was purchased from Alfa Aesar, Poly(vinylpyrrolidone) (PVP), MW = 58000, AR) was purchased from Sinopharm Chemical Reagent Co. Ltd. (Shanghai, China). All reagents were used as received without further purification.

2.2. Synthesis

2.2.1. Synthesis of Graphene Oxide

The catalyst support, reduced graphene oxide (GO), was prepared through the reduction of graphite by $NaBH_4$. The graphene oxide (GO) was prepared by the modified Hummers method [23]. In a typical experiment 2 g of graphite powder was first added into 100 mL concentrated H_2SO_4 at room temperature. Under stirring, the mixture was cooled to 5°C using an ice bath, and the temperature of the mixture was kept to be below 5°C for 30 min. 8 g $KMnO_4$ was then added gradually under stirring and cooling, so that the temperature of the mixture was not allowed to reach 10°C. 100 mL distilled water was added into the mixture, stirred for 1 h, and further diluted to approximately 300 mL with distilled water. After that, 20 mL of 30% H_2O_2 was added to the mixture to reduce the residual $KMnO_4$. The solid was filtered, washed with 5% HCl aqueous solution to remove metal ions and with distilled water until the pH was 6. The resulting graphite oxide was dried at 50°C for 24 h.

2.2.2. Synthesis of Pd Octahederal Nanocrystals on Graphene Oxide

Above synthesized GO powder was dispersed in water (1mg/1mL) and ultrasonicated for 30 minutes. Then 105 mg of PVP as capping agent and 1 mM of H_2PdCl_4 solution was added in GO dispersion. Reaction flask was sealed to create high vacuum environment and heated up to $95\ ^0$C with continuous stirring and bubbling of H_2 as reducing agent for 30 minutes. The resulting products were collected by centrifugation and washed several times with ethanol and acetone to remove excess amounts of PVP from nanocrystals. Pd octahedral nanocrystals are demonstrated as GO/Pd-01 in all the figures.

2.2.3. Synthesis of Pd Spherical Nanocrystals on Graphene Oxide

For spherical nanocrystals the synthesis procedure is exactly the same as above for octahedral nanocrystals but only the difference is CO gas is used as a reducing agent instead of H_2. Pd spherical nanocrystals are demonstrated as GO/Pd-02 in all the figures.

2.3. Characterization Tools

2.3.1. Physical Characterization

After synthesis of GO, its characterizations were done to make sure the 2D structure of GO sheets, presence of C-C / C-H / C-OH bonds, characteristics of GO with transmission electron microscopy (TEM), fourier transform infrared spectroscopy (FTIR) and UV-Vis spectroscopy, respectively. Then after synthesis of Pd nanocrystals on GO, their physical characterizations were done by scanning electron microscopy (SEM), the powder X-ray diffraction (XRD) measurements were performed with an X'pert PRO instrument (PANalytical) using CuKα radiation (λ = 0.15418 nm) and UV-Vis spectroscopy within the range of 200 to 800nm.

2.3.2. Electrochemical Characterization

Before each electrochemical experiment, a glassy carbon (GC) electrode (0.196 cm^2 geometric surface area) was first polished with alumina slurries (Al_2O_3, 0.05 μm) on a polishing cloth to obtain a mirror finish, followed by sonication in 0.1 M HNO_3, 0.1 M H_2SO_4, and pure water for 10 min, successively. To prepare a cata-

lyst-coated working electrode, 15 μL of the 1 mg/mL suspension in pure water was drop-coated on the polished electrode surface by a microliter syringe, followed by drying in vacuum at room temperature. Afterward, the catalyst was covered with a thin layer of Nafion (0.1 wt % in water, 5 μL) to ensure that the catalyst was tightly attached to the electrode surface during the electrochemical measurements. Voltammetry measurements were carried out with a CHI750D electrochemical workstation. The electrode prepared above was used as the working electrode. The Ag/AgCl (in 3 M NaCl, aq.) combination isolated in a double junction chamber and a Pt coil were used as the reference and counter electrodes, respectively. All the measurements were performed in electrochemical experiments with respect to standard values of reversible hydrogen electrode (RHE). Electrochemical characterizations were done by cyclic voltammetry (CV), linear sweep voltammetry (LSV) and chronoamperometry (CA).

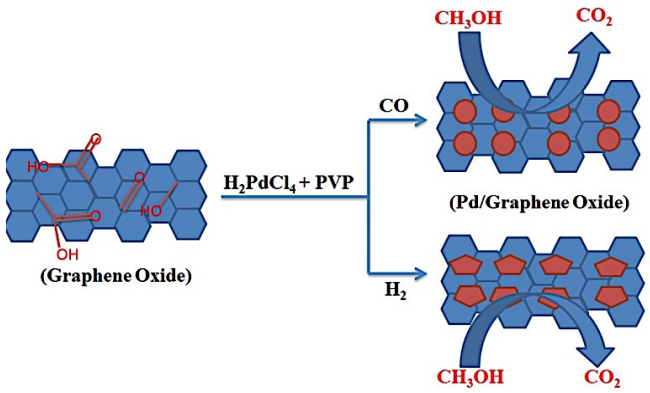

Figure 1. Schematic representation of the synthesis procedure of the GO/Pd hybrid catalysts.

3. RESULTS AND DISCUSSION

A facile synthetic route is applied to prepare GO/Pd hybrid composites with different shape Pd nanocrystals as illustrated in the schematic diagram in Figure 1. For this purpose, we initially prepare GO via the Hummer's method and then reduce it by $NaBH_4$. Since GO contains a large number of oxygen-containing functional groups, which allow GO to be well dispersed in an aqueous solution [24,25]. Their functional group presence is analyzed from FTIR spectra given in Figure S1-b. The graph shows the stretching of hydroxyl group at 3450 cm^{-1}, the C=O carbonyl stretching at 1728 cm^{-1}, and the C-O epoxide group stretching at 1229 and 1061 cm^{-1} [26]. The high intensity of the main peaks in GO confirms the presence of large amount of oxygen functional groups after the reduction process. The morphology of sheet structure of GO is analyzed from TEM shown in Figure S1-a. The reduced graphene oxide exhibit typical wrinkled structure that caused sheet folding [27]. This 2D structure of GO and presence of oxygen-containing functional groups not only increases the specific contact area, which facilitates the transport of the Pd ions and electrons into the inner region of the graphene sheets, but also provides more exposed active sites for the anchoring of Pd precursors and Pd nucleation [28].

The formation of GO/Pd hybrid composite is based on the nucleation and growth of spherical and octahedral Pd nanocrystals on the suitable surface sites of GO through a capping agent PVP and by the reduction of H_2PdCl_4 through H_2 and CO. As a typical surface-capping agent PVP is generally added at the start of the reaction or continuously during metal reduction. The role of the PVP is dual: it acts as a stabilizing agent, preventing aggregation of metal particles and retaining a uniform colloidal dispersion. Moreover, PVP is used as a shape-control agent or crystal-habit modifier, promoting reduction onto specific crystal faces while inhibiting reduction onto others [29]. PVP has been demonstrated to stabilize the lowest energy crystal facets of noble metals having fcc crystal system. PVP binds preferentially to the {111} and {110} planes. In our case, we have found that the presence of PVP is important for stabilizing, as well as in controlling the decoration of Pd nanocrystals. The role of CO and H_2 gas include reduction of metal precursors and binding of different facets to make different shape noble metal nanocrystals. In the case of Pd spherical nanocrystals, the CO-Pd (111) system has been widely studied over the last decade. Experimentally, a set of ordered CO adsorption patterns have been determined [30,31]. It has been known that CO adsorbs preferentially onto specific surfaces of various metals [32,33]. Besides, the effect of capping agents, this selective binding could help the preferred addition of more Pd atoms onto given facets of Pd nanocrystals, because CO can undergo preferential oxidation to CO_2 on selected surfaces [34,35]. For the transition state, the absorbed CO molecules on the {100} surfaces are slightly more stretched and closer to the surface than those over the {111} surfaces [35]. Adsorption of CO on Pd atoms is stronger on the {100} surfaces than the closely packed {111} surfaces. This deviancy could lead to the difference in the potential energy of the transition state for the adsorbed CO on these two surfaces [35-37]. Since the oxidation yields gas phase byproducts, much less perturbation to the synthetic mixture is expected than those with soluble liquid or solid reductants. Thus, stable reduction and other local reaction environments should be sustained using the liquid solution approach.

In the case of Pd Octahedral nanocrystals, the mechanism of H_2 adsorption as reducing agent in the presence of a stabilizing agent (PVP) is a key point of discussion for this work. CO-H interaction on Pd (111) surface has attracted much attention for the researchers [38,39]. Fu *et al.,* have discussed the co-adsorption of CO and H_2 on Pd (111) surface. Their main conclusion was that CO co-adsorption would cause adsorbed H atoms desorbing as H_2 or dissolving into a Pd lattice. Morkel *et al.,* additionally pointed that for Pd nanoparticles, a hydride phase is more easily formed, and dissolved hydrogen starts to desorb only after a considerable amount of CO has been removed [40]. According to the neutron diffraction experiment [39,40], H atoms locate on the octahedral position in the bulky Pd lattice, with a saturation concentration of $x \approx 0.64$. From H_2 interaction, two different hydrogen adspecies appear on the surface of Pd in the process of formation of PdH_x. The negatively polarized atomic adspecies, being formed at the beginning of the process, denoted to as β^-, and the positively polarized atomic adspecies, arising with the increasing coverage, denoted as β^+. However the β^- seems to be stable on the surface, the β^+ incorporated quickly into the bulk forming hydrides. So upon bubbling with H_2, Pd nanosheets were converted into Pd hydride, PdH_x. Pd (111) surface is partially saturated by the interstitial H atom, which

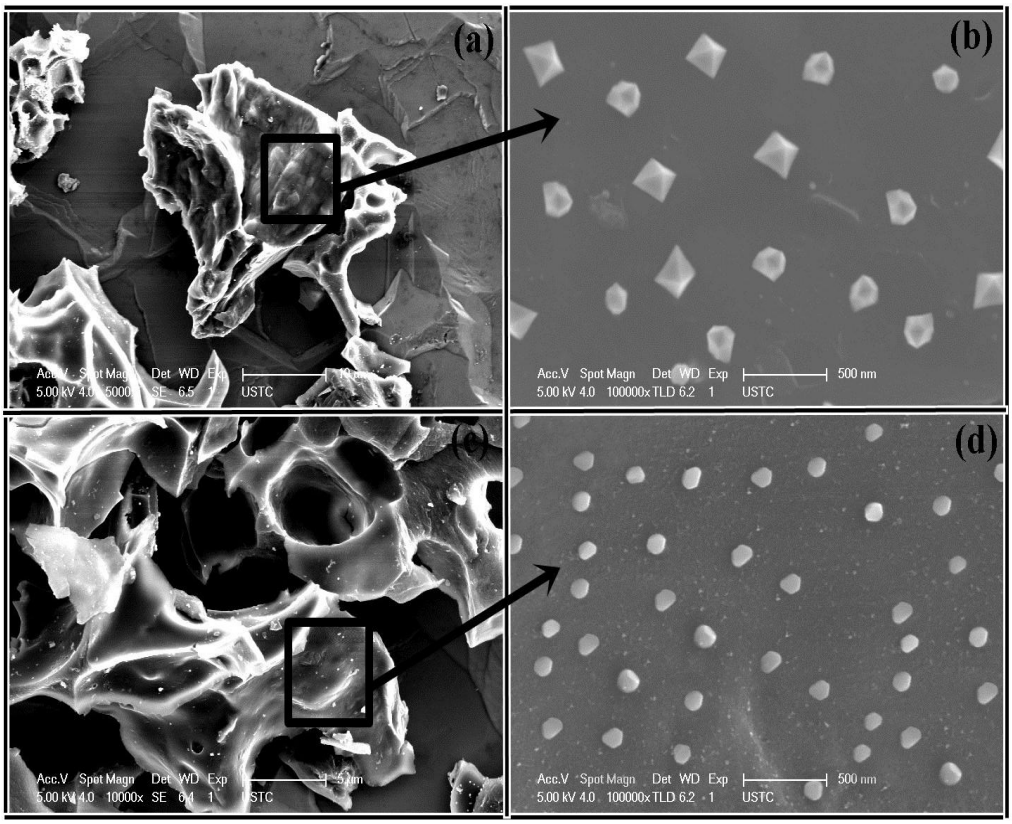

Figure 2. FE-SEM images of Pd nanocrystals on crumpled GO (left side), High magnifications images of Pd Octahedral and Pd Spherical nanocrystals on crumpled GO (right side).

become energetically stable. This creates the seed growth of the small nanosheets on the GO sheets. The increased thickness of the nanosheets resulted by the deposition of Pd atoms on Pd(111) surface by an atomic addition process allowed by the presence of H_2. As the H atoms occupy octahedral sites, so the atomic addition process eventually leads to the synthesis of Pd octahedral nanocrystals from initially grown Pd nanosheets of (111) facets.

FESEM images of the samples GO/Pd-01 and GO/Pd-02 are shown in Figure 2. The FESEM images revealed that Pd spherical and octahedral nanocrystals with a uniform size were well-dispersed on the surfaces of the GO. It was clearly shown in FE-SEM micrographs that spherical and octahedral Pd nanocrystals were the dominant phases. The high-magnification FE-SEM image shows that Pd octahedrons have well-defined shapes with a uniform size distribution (Figure 2a). It can be seen that the prepared Pd nanocrystals are uniformly distributed on the GO surface. It should be noted that almost no Pd nanocrystals can be observed outside the GO sheet, indicating that GO serves here as a template for the Pd nanocrystals formation. As shown in Figure 2b, spherical Pd nanoparticles were deposited onto the surface of GO with greater retention of the spherical characteristics of the nanocrystals.

The obtained GO/Pd composite was characterized by a UV-Vis absorption spectrum to confirm the existence of Pd nanocrystals loaded on GO as shown in Figure 3. In the absorption spectrum of reduced GO, the broad absorption peak centered around 270nm can be ascribed to the π−π* transitions of aromatic C=C bonds. For the GO/Pd hybrid composite, no obvious absorption peak was observed, showing a typical Mie exponential decay profile [41].

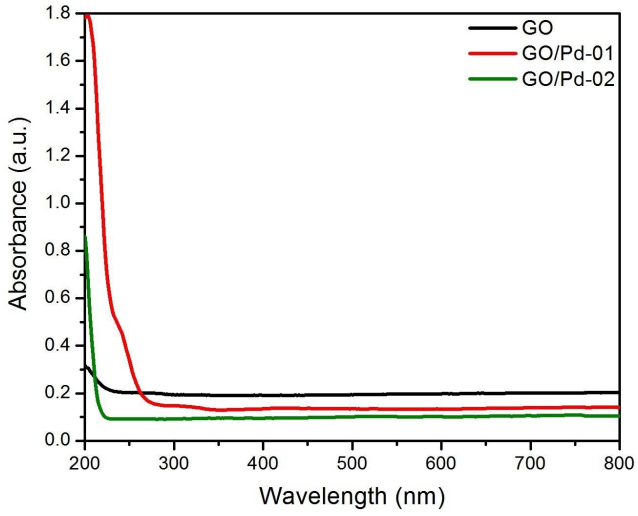

Figure 3. UV-vis spectra of Pd Octahedral (GO/Pd-01) and Pd Spherical (GO/Pd-02) nanocrystals.

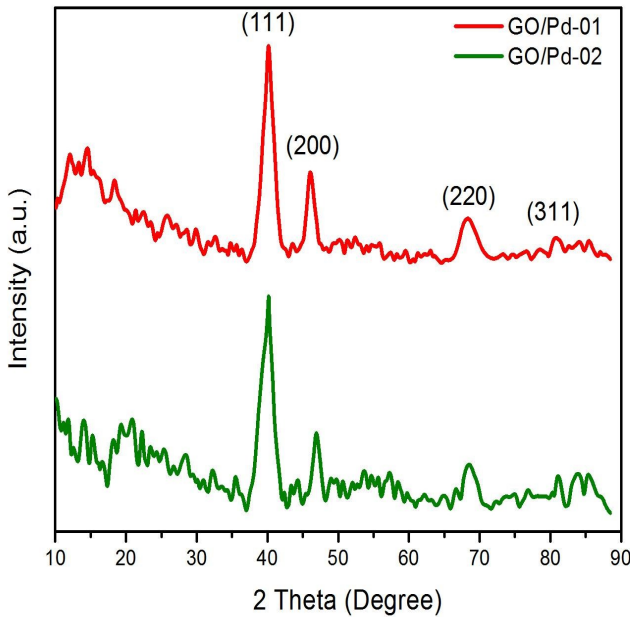

Figure 4. XRD spectra of Pd octahedral (GO/Pd-01) and Pd spherical (GO/Pd-02) nanocrystals.

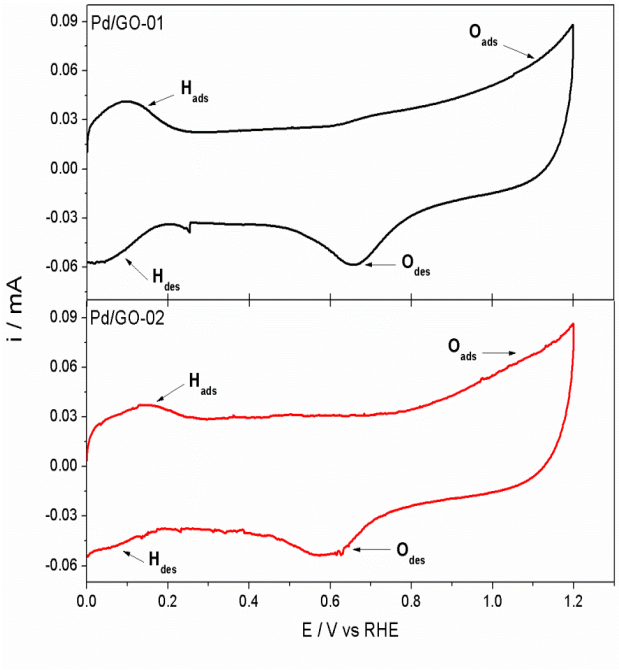

Figure 5. LSV peaks of Pd octahedral (GO/Pd-01) and Pd spherical (GO/Pd-02) nanocrystals after CO-stripping cleaning treatment, in 0.1M $HClO_4$ at scan rate of 50 mV/s vs RHE.

GO/Pd composite was further characterized by XRD to investigate the hybrid. As shown in Figure 4, the XRD pattern of Pd/GO-1 and Pd/GO-2 composites, diffraction peaks at 40.20°, 46.87°, 68.56° and 81.93° are ascribed to the (111), (200), (220) and (311) crystalline planes of the face centered cubic (fcc) structure of Pd, respectively. The diffraction peaks are consistent with a fcc crystalline structure of bulk Pd (JCPDS, card no. 46-1043). The relatively broad diffraction peak observed at 10° to 30° centered at $2\theta = 24.5°$ corresponds to the (002) plane of graphene. It is an eminent fact that metallic Pd is catalytically active to split H_2 molecules to hydrogen atoms which can completely permeate into Pd to form metal hydride [42-44]. In fact, the powder XRD measurements (Figure 4) on the freshly prepared Pd nanocrystals confirmed that the as-prepared octahedrons and spherical nanocrystals are completely metallic and there is no evident peak observed for β-PdHx. This may be due to the high vacuum environment and temperature that all the transition phases of Pd are converted into a metallic phase Pd. The crystallite size of the particles was also calculated from XRD data by using Debye Scherrer's formula (Table S1). The average crystal size calculated by XRD is closely co-related with the SEM measurements; hence both the results can strengthen each other's accuracy.

The electrochemical properties of Pd/GO hybrid composites were examined by measuring cyclic voltammograms (CVs). Before observing the electrochemical behavior of the catalysts, they were cleaned by three different methods. Because the metal surface capped with organic ligands, which served as capping agents, largely reduce their catalytic activity when they are used as catalysts. In the past few years, various methods have been applied to clean or remove these surfactants, such as thermal annealing, acetic acid washing, oxygen plasma cleaning, and UV-ozone irradiation. However, these methods require either extremely high temperature or long treatment time. At the same time, the cleaning process may cause the change in particle size and morphology, especially for the shaped nanocrystals. Therefore, it is essential to develop a simple and effective strategy to clean the surface of nanoparticles and make them catalytically active. Here, we demonstrate that CO-stripping is an efficient method to clean the particle surface over oxygen plasma cleaning and simple electrochemical cleaning and thus improve the electrocatalytic activity of the PVP- stabilized Pd nanocrystals. Figure S2 and Figure S3 show the CVs of the Pd octahedral and spherical nanocrystals supported on a glassy carbon electrode respectively, after electrochemical, oxygen plasma and CO-stripping treatments. These base CVs are restricted in a small region between 0 to 1 V in order to avoid for the destruction of electrode at many scanes cycles. Compared to the all three treatments, the CO stripping-treated electrode exhibited clearer hydrogen region and oxygen region and eventually an increased electrochemically active surface area (ECSA), which further can enhance catalytic activity towards methanol oxidation. Finally, more surface atoms were exposed and became electrochemically active after CO stripping which is also characterized by CV at longer scale from 0.05 to 1.2V vs RHE where oxidation reductions peaks are clearly visible which is given in Figure 5. The present result is similar to that of another recent study where the CO treated cleaned PtPd/RGO catalyst and surfactant-free Ag nanorods exhibited good characteristic CV and much enhanced electrocatalytic activity compared with the PVP-stabilized ones [45-47].

In order to calculate the electrochemical active surface area (ECSA), the cyclic voltammograms (CVs) curves of GO/Pd-01 and GO/Pd-02 presented in Figure 5. As shown in these voltamograms,

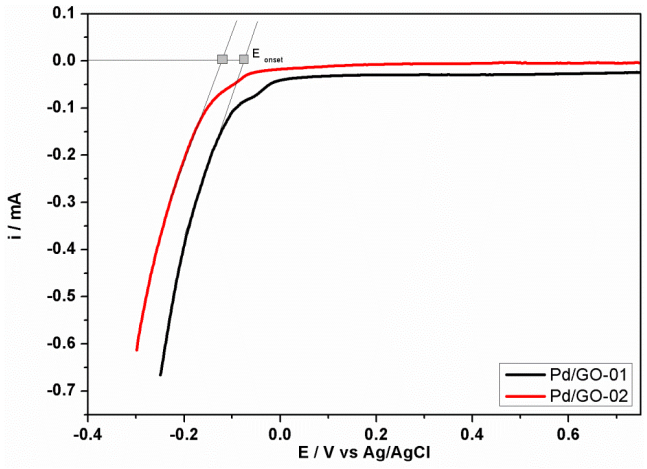

Figure 6. Polarization curves for HER activity of Pd octahedral (GO/Pd-01) and Pd spherical (GO/Pd-02) nanocrystals in 0.1 mol L^{-1} $HClO_4$ at a san rateof 10 mV s^{-1} vs Ag/AgCl. E_{onset} for HER is measured by tangent method.

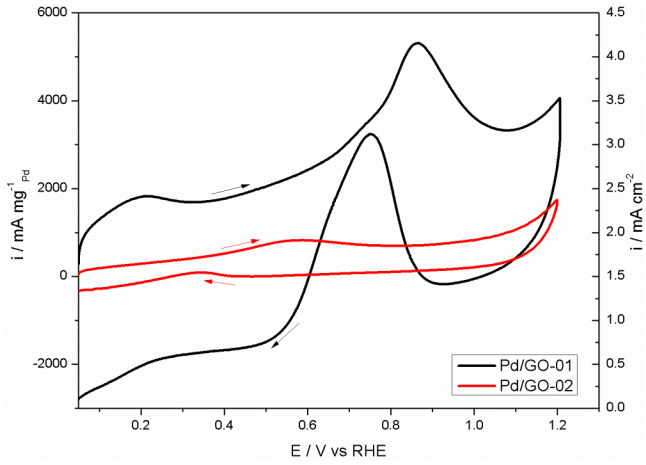

Figure 7. MOR activity peaks (forward and backward scans) of Pd octahedral (GO/Pd-01) and Pd spherical (GO/Pd-02) nanocrystals in 0.1 mol L^{-1} $HClO_4$ + 1 mol L^{-1} CH_3OH at a san rate of 50 mV s^{-1} vs RHE.

there is hydrogen adsorption/desorption region (0.05-0.3 V) and surface metal oxidation/reduction region (0.4-0.8 V) on the CV curves for all the catalysts. From these CVs, their ECSAs were determined by integrating the area bounded by the hydrogen adsorption curve and the baseline in the range of 0.05-0.4 V (Table 1). The detailed calculation with appropriate formula and method are also provided in Supplementary information (S1). The increase in ECSA of octahedral NCs than spherical NCs should be attributed to optimize dispersion and size distribution of the octahedral NCs on GO, which can further improve the electrocatalytic activity of octahedral NCs.

The enhancement factor for electrocatalytic activity of octahedral NCs over spherical NCs is also measured theoretically from surface area to volume (S/V) ratio concepts of bulk materials. As for the bulk material S/V values are slightly higher for octahedral crystals than the spherical crystals by a factor of 1.15, which can lead to the enhancement of surface properties of octahedral crystals than the spherical. In case of nanoparticles S/V values have significant effect on their properties. As the S/V values increases with the decrease in crystallite size of the material. Therefore as particle size decreases, a greater portion of the atoms are found at the surface compared to those inside. Therefore, nanoparticles have much greater surface area per unit volume compared with the larger particles. It leads to nanoparticles more chemically reactive. As growth and catalytic chemical reaction occurs at surfaces, therefore a given mass of nanomaterial will be much more reactive than the same mass of material made up of large particles. It is also found that materials which are inert in their bulk form are reactive when produced in their nanometric scale. It can improve their properties.

In our studies the granulometric data obtained from SEM is used to calculate S/V values of NCs, calculated in the Supplementary information (S2). The S/V value for octahedral NCs is higher than that of spherical NCs by a factor of 1.2 which is slightly higher and nearly equal to the bulk calculated value. This enhancement in S/V for octahedral NCs can explain the enhancement in their electrocatalytic properties and enhancement of S/V factor value over bulk material can explain the nano sized confirmation of NCs with higher surface catalytic properties over bulk materials.

HER perfomance is presented here in Figure 6. The onset potential is measured by tangent method. From the figure, it is clear that the onset potential for evolution of adsorbed hydrogen on the surface active sites of the catatalyst is more near towards zero for octahedral NCs than that of spherical NCs. This confirms that octahedral NCs could show better performance as anode material for DMFCs. This argument is further proved by MOR measurements.

The electro activity of Pd spherical and octahedral nanocrystals towards methanol oxidation in 0.1 mol L^{-1} $HClO_4$+1 mol L^{-1} CH_3OH solution at a scan rate of 50 mV s^{-1} are demonstrated in Figure 7. The current density is normalized to the geometric surface area to make a comparison of the two catalysts loaded on same diameter sized GCE. At potentials below 0.40 V to 0.30 V, the oxidation current is lower, but not negligible in all voltammograms because the surface active sites are poisoned by CO_{ads}, an interme-

Table 1. Comparison of ECSA and current density values for both the catalysts w.r.t different parameters.

Catalyst	ECSA cm^{-2}	ECSA cm^{-2}_{Pd}	J^a	J^b	J^c	J^d
GO/Pd-01	0.245	8.3	4.3	3.56	100	5300
GO/Pd-02	0.067	2.2	2.0	1.95	60	1800

J^a = $mA.cm^{-2}$ w.r.t GSA, J^b = $mA.cm^{-2}$ w.r.t ECSA, J^c = $\mu A.cm^{-2}_{Pd}$ w.r.t ECSA, J^d = $mA.mg^{-1}_{Pd}$ w.r.t mg^{-1}_{Pd}

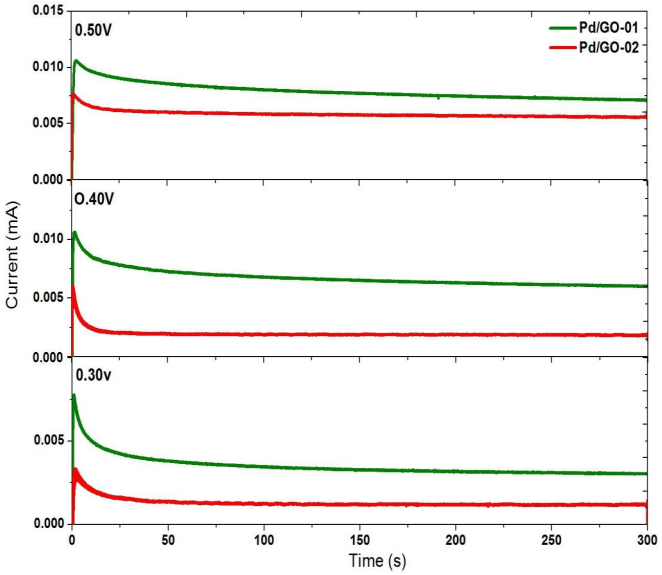

Figure 8. CA results of MOR activity for Pd octahedral (GO/Pd-01) and Pd spherical (GO/Pd-02) nanocrystals in 0.1 M $HClO_4$ + 1M CH_3OH at constant voltage 0.30 V, 0.40 V and 0.50 V up to 300s time.

diate from dehydrogenation of methanol. With the potential increasing, the oxidation current takes off rapidly, representing that significant methanol oxidation occurs. The current densities obtained from different aspacts such as with respect to ECSA, Geometric surface area (GSA), actual loading of Pd metal to geometric surface area and real loading of Pd metal to ECSA are compared for both the catalysts (Table 1). This increase of oxidation current is also characterized by CA measurements up to 300s at constant potentials of 0.30 V, 0.40 V and 0.50 V demonstrated in Figure 8. This CA measurement clearly showing the increase of oxidation current from lower potential to higher potential with maximum stability for 300s for both the catalysts. Onset potential and current density are the two major parameters to evaluate the catalytic activity of electro catalysts. The onset potential of both the catalysts is obtained at 0.30 V vs RHE. But the current density at onset potential for Pd octahedral nanocrystals is higher than that of Pd spherical nanocrystals, which is characterized by CA measurements. The maximum current density at positive potential or forward current is obtained for the Pd octahedral catalyst at ca. 4.5 mA cm^{-2} (specific activity), ca. 5300 mA mg^{-1}_{Pd} (mass activity) and for Pd spherical catalyst at ca. 2 mA cm^{-2} (specific activity), ca. 1800 mA mg^{-1}_{Pd} (mass activity) [48]. These results indicate that Pd octahedral offers a high electrocatalytic activity towards methanol oxidation than Pd spherical nanocrystals. The reason is that in Pd octahedral nanocrystal (111) facets are more abundant and exposed to the surface to catalyze the methanol molecules more effectively than Pd spherical nanocrystals. In Pd octahedral nanocrystals the edges and corners of octahedral geometry are also effectively important for the oxidation of formic acid into CO_2 [49]. As the formic acid is one of the intermediate in the electro oxidation mechanism of methanol. This intermediate is also catalyzed by octahedral nanocrystals but on the other hand, spherical nanocrystals became unable to oxidize this intermediate rapidly and ultimately which terminate the further oxidation of methanol.

5. CONCLUSIONS

In conclusion, palladium octahedral and spherical nanocrystals with uniform morphology were successfully synthesized in the presence of hydrogen and carbon monoxide, respectively. The as made Pd nanocrystals are bound with {111} facets. The electrocatalytic activity as an anode material for DMFCs with comparative study shows that Pd octahedral nanocrystals have good affinity towards methanol oxidation with an improved catalytic activity over that of Pd spherical nanocrystals of similar facets, which was formerly characterized and proved by HER performance for both the nanocrystals. The current work, not only gives a simple method to synthesize Pd nanocrystals with special facets on graphene oxide, but also offers a comparative analysis among both NCs. Together with the use of specific strong adsorbates to control the surface structure of Pd nanocrystals, the shape-control strategy, hydrogen evolution reaction activity and methanol oxidation reaction active catalyst reported here could provide a new research avenue to further enrich the Pd based nanocrystals.

6. SUPPLEMENTARY INFORMATION

S1. Measurement of Electrochemical Active Surface Area (ECSA)

$A = \frac{Q_H}{Q_H^*}$ gives the electrochemically accessible area of Pd in the electrode

where Q_H^* = 212μC/cm^2; $Q_H = \frac{\int i \cdot dE}{v}$

Scan rate (υ) =50mv/s

$\int i \cdot dE$ is the area from the hydrogen desorption region given in the following figures.

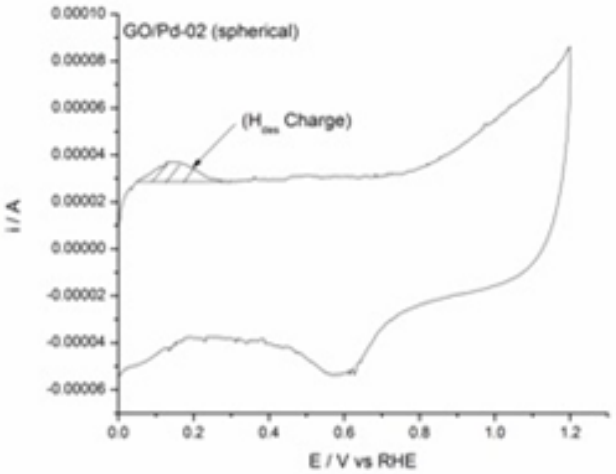

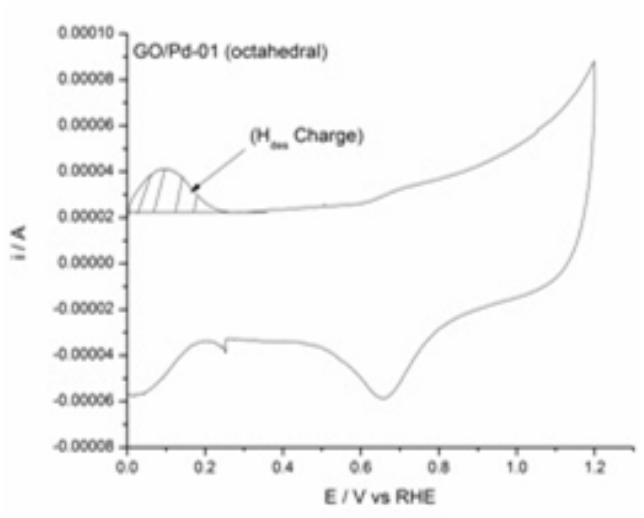

a. For GO/Pd-01 (Octahedral NPs)

$$\int i \cdot dE = \cdots A \cdot V \therefore \frac{\int i \cdot dE}{v} = \frac{2.6E^{-06} A \cdot V}{0.05 V/s} = 0.000052 A \cdot s = 0.000052 C$$

$$A_{real} = \frac{Q_H}{Q_H^*} = \frac{(0.000052C)(1x10^6 \mu C)}{(212 \mu C/cm^2_{real})\,(1C)} = 0.245 cm^2$$

$$\therefore Pd\ loading = \left(1 \frac{mg}{cm^2_{geo}}\right)(geometric\ area\ of\ the\ work\ electrode, 0.196 cm^2)(15\%)$$
$$= 0.0294 mg\ Pd$$

$$ESA = \frac{0.245 cm^2_{real}}{0.0294 mg_{Pd}} = 8.3 \frac{cm^2_{real}}{mg_{metal}}$$

b. For GO/Pd-02 (Spherical NPs)

$$\int i \cdot dE = 7.2E^{-07} A \cdot V \therefore \frac{\int i \cdot dE}{v} = \frac{7.2E^{-07} A \cdot V}{0.05 V/s} = 0.00000144 A \cdot s = 0.00000144 C$$

$$A_{real} = \frac{Q_H}{Q_H^*} = \frac{(0.00000144C)(1x10^6 \mu C)}{(212 \mu C/cm^2_{real})\,(1C)} = 0.067 cm^2$$

$$\therefore Pd\ loading = \left(1 \frac{mg}{cm^2_{geo}}\right)(geometric\ area\ of\ the\ work\ electrode, 0.196 cm^2)(15\%)$$
$$= 0.0294 mg\ Pd$$

$$ESA = \frac{0.067 cm^2_{real}}{0.0294 mg_{Pd}} = 2.2 \frac{cm^2_{real}}{mg_{metal}}$$

S2. Measurement of Specific Surface area to Volumen Ratio (and a Factor) from Granulometric Data of Octahedral and Spherical NPs

a. For GO/Pd-01 (Octahedral NPs)

$$S_{oct} = 2a^2\sqrt{3}$$

$$V_{oct} = \frac{1}{3} a^3 \sqrt{2}$$

$$\frac{S_{oct}}{V_{oct}} = \frac{3\sqrt{6}}{a}$$

a = 34 nm (average edge length obtained from SEM granuolometric data)

$$\frac{S_{oct}}{V_{oct}} = 0.21$$

b. For GO/Pd-01 (Spherical NPs)

$$S_{sphere} = 4\pi a^2$$

$$V_{sphere} = \frac{4}{3} \pi a^3$$

$$\frac{S_{sphere}}{V_{sphere}} = \frac{3\sqrt{6}}{a}$$

a = 33 nm (average edge length obtained from SEM granuolometric data)

$$\frac{S_{oct}}{V_{oct}} = 0.17$$

From above obtained values the specific surface area of octahedral NPs is slightly higher than that of spherical NPs (by a factor of 1.2).

7. ACKNOWLEDGMENTS

Majid Khan and Ammar Bin Yousaf contributed equally to this work. This work is supported by China Scholarship Council (CSC) and USTC fellowship programme offered by University of Science and Technology of China, Hefei, and Anhui Government Scholarship offered by Anhui Provincial Government of China.

REFERENCES

[1] T. K. Sau, A. L. Rogach, F. Jackel, T. A. Klar, J. Feldmann, Adv. Mater., 22, 1805 (2010).
[2] A. R. Tao, S. Habas, P. Yang, Small, 4, 310 (2008).
[3] T. Teranishi, M. Hosoe, T. Tanaka, M. Miyake, J. Phys. Chem. B, 103, 3818 (1999).
[4] M. Khan, A. B. Yousaf, M. Chen, C. Wei, X. Wu, N. Huang, Z. Qi, L. Li, J. Power Sources, 282, 520 (2015).
[5] Y. N. Xia, Y. J. Xiong, B. Lim, S. E. Skrabalak, Angew. Chem. Int. Ed., 48, 60 (2009).
[6] T. K. Sau, A. L. Rogach, Adv. Mater., 22, 1781 (2010).
[7] Z. Y. Zhou, N. Tian, J. T. Li, I. Broadwell, S. G. Sun, Chem. Soc. Rev., 40, 4167 (2011).
[8] D. Astruc, F. Lu, J. R. Aranzaes, Angew. Chem., Int. Ed., 44, 7852 (2005).
[9] R. Narayanan, M. A. El-Sayed, J. Phys. Chem., 109, 12663 (2005).
[10]Z. M. Peng, H. Yang, Nano Today, 4, 143 (2009).

Table S1: Measurement of crystallite size from XRD data using Debay-Sherrer Equation

Phase	Width	2θ (deg)	(hkl)	Particle size (nm)
GO/Pd-01 Octahedral NPs	2.36	40.1	111	40.11
	1.98	46.7	200	34.37
	1.40	68.1	220	26.88
GO/Pd-02 Spherical NPs	2.26	40.1	111	38.30
	1.94	46.7	200	33.70
	1.38	68.1	220	26.51

Average crystallite size for GO/Pd-01 = 33.78
Average crystallite size for GO/Pd-02 = 32.83

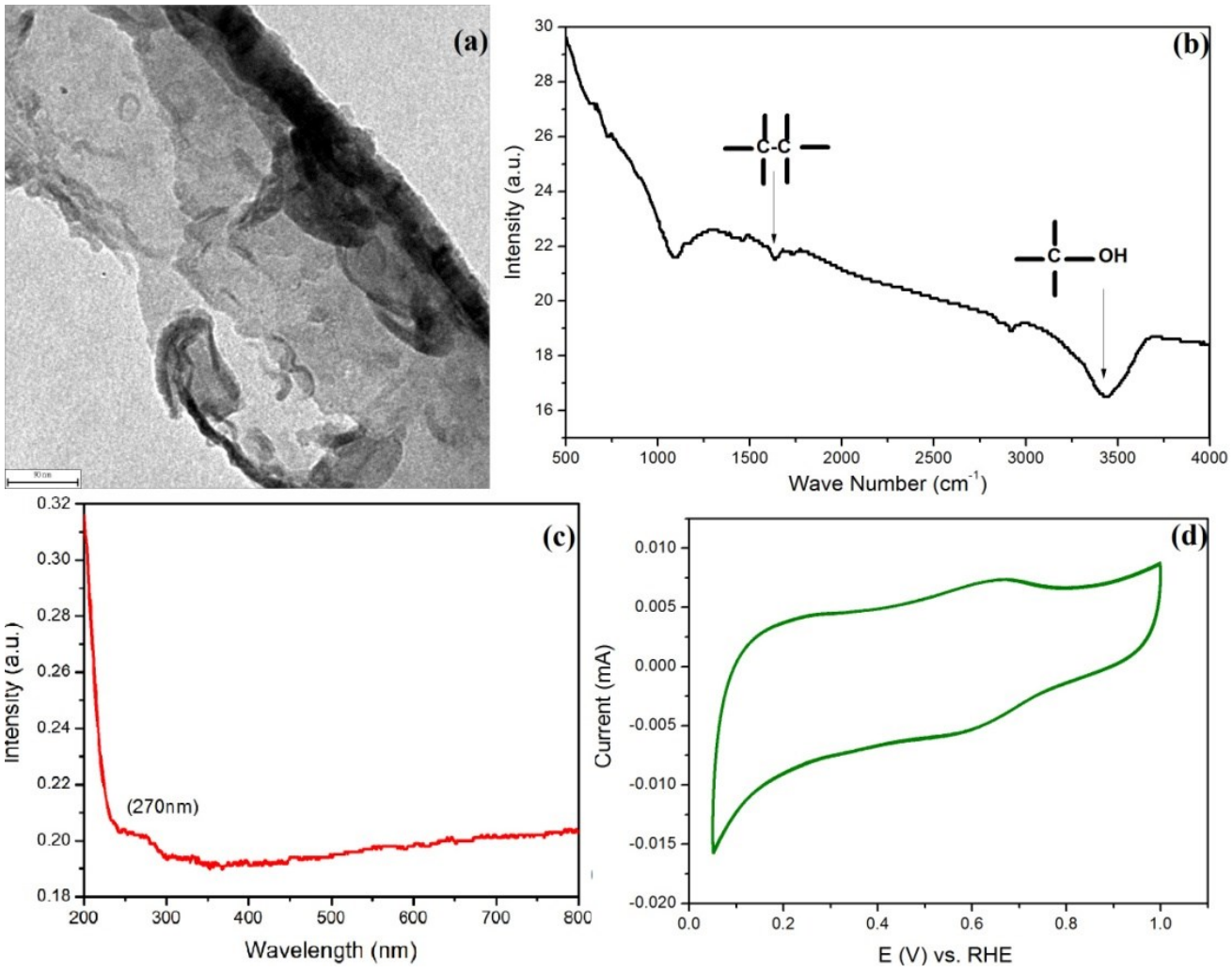

Figure S1: Characterizations of synthesized Graphene Oxide (a) TEM image, (b) FTIR spectrum, (c) UV-vis spectrum and (d) CV in 0.1 mol.L^{-1} $HClO_4$ at a scan rate of 50 mV.s^{-1} vs RHE.

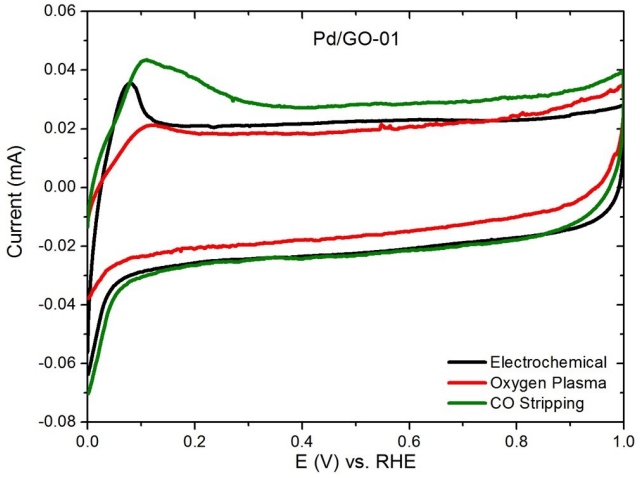

Figure S2: CVs of Pd octahedral (GO/Pd-01) nanocrystals after different cleaning treatments, in 0.1 mol.L^{-1} $HClO_4$ at a scan rate of 50 mV.s^{-1} vs RHE.

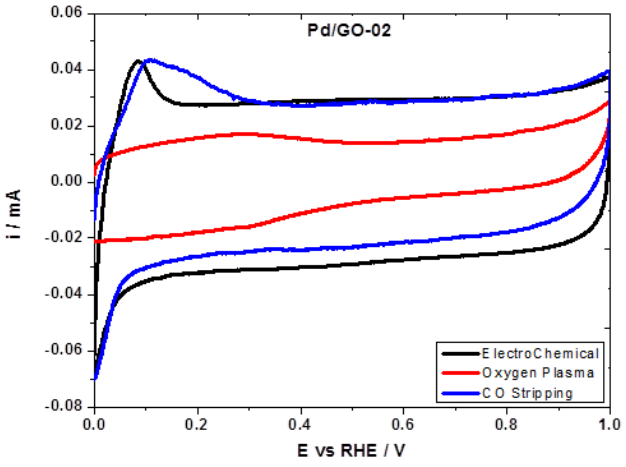

Figure S3: CVs of Pd spherical (GO/Pd-02) nanocrystals after different cleaning treatments, in 0.1 mol.L^{-1} HClO4 at 50 mV.s^{-1} vs RHE.

[11]Y. Sun, Y. Xia, Science, 298, 2176 (2002).
[12]H. Zhang, M. Jin, Y. Xia, Angew. Chem., Int. Ed., 51, 7656 (2012).
[13]M. Chen, B. Wu, Y. Yang, N. Zheng, Adv. Mater., 24, 862 (2012).
[14]X. Huang, S. Tang, H. Zhang, Z. Zhou, N. Zheng, J. Am. Chem. Soc., 131, 13916 (2009).
[15]T. K. Sau, A. L. Rogach, Complex-shaped Metal Nanoparticles: Bottom-up Synthesis and Applications, John Wiley & Sons, Germany, 2012.
[16]L. D. Rampino, F. F. Nord, J. Am. Chem. Soc., 63, 2745 (1941).
[17]W. Zhang, X. Chen, R. A. Boulos, J. Toster, C. L. Raston, Chem. Comm., 50, 15167 (2014).
[18]B. Wu, N. Zheng, G. Fu, Chem. Commun., 47, 1039 (2011).
[19]G. Chen, Y. Tan, B. Wu, G. Fu, N. Zheng, Chem. Commun., 48, 2758 (2012).
[20]Y. Xiong, Y. Xia, Adv. Mater., 19, 3385 (2007).
[21]X. Huang, S. Tang, X. Mu, Y. Dai, G. Chen, Z. Zhou, F. Ruan, Z. Yang, N. Zheng, Nat. Nanotechnol, 6, 28 (2011).
[22]X. Huang, S. Tang, J. Yang, Y. Tan, N. Zheng, J. Am. Chem. Soc., 133, 15946 (2011).
[23]Y. Dai, X. Mu, Y. Tan, K. Lin, Z. Yang, N. Zhen, G. Fu, J. Am. Chem. Soc., 134, 7073 (2012).
[24]W. S. Hummers, R. E. Offeman, J. Am. Chem. Soc., 80, 1339 (1958).
[25]M. Khan, A. B. Yousaf, M. Chen, C. Wei, X. Wu, N. Huang, Z. Qi, L. Li, Nano Res., 9, 837 (2016).
[26] S. Thakur, N. Karak, Carbon, 50, 5331 (2012).
[27] H. Zhang, P. X. Feng, Carbon, 48, 359 (2010).
[28]X. M. Chen, G. Wu, J. Chen, X. Chen, Z. Xie, X. Wang, J. Am. Chem. Soc., 133, 3693 (2011).
[29]Y. J. Song, M. Wang, X. Y. Zhang, J. Y. Wu, T. Zhang, Nanoscale Res. Lett., 9, 17 (2014).
[30]M. Tushaus, W. Berndt, H. Conrad, A. M. Bradshaw, B. Persson, Appl. Phys. A: Mater. Sci. Process, 51, 91 (1990).
[31]M. K. Rose, T. Mitsui, J. Dunphy, A. Borg, D. F. Ogletree, M. Salmeron, P. Sautet, Surf. Sci., 512, 48 (2002).
[32]E. Herrero, K. Franaszczuk, A. J. Wieckowski, Phys. Chem., 98, 5074 (1994).
[33]S. Schauermann, J. Hoffmann, V. Johanek, J. Hartmann, J. Libuda, H. J. Freund, Angew. Chem., Int. Ed., 41, 2532 (2002).
[34]Z. M. Peng, H. J. You, H. Yang, ACS Nano, 4, 1501 (2010).
[35]A. Eichler, Surf. Sci., 498, 314 (2002).
[36]C. J. Zhang, P. J. Hu, J. Am. Chem. Soc., 123, 1166 (2001).
[37]G. A. Somorjai, Y. Li, Introduction to Surface Chemistry and Catalysis, 2nd ed.; John Wiley & Sons, Hoboken, NJ, 2010.
[38]M. Morkel, G. Rupprechter, H. J. Freund, Surf. Sci., 588, 209 (2005).
[39]J. I. Cerda, B. Santos, T. Herranz, J. M. Puerta, J. Figuera, K. F. McCarty, J. Phys. Chem. Lett., 3, 87 (2011).
[40]J. E. Worsham, M. K. Wilkinson, C. G. Shull, J. Phys. Chem. Solids, 3, 303 (1957).
[41]W. Chen, J. R. Davies, D. Ghosh, M. C. Tong, J. P. Konopelski, S. W. Chen, Chem. Mater., 18, 5253 (2006).
[42]W. Palczewska, Adv. Catal., 24, 245 (1975).
[43]M. V. Goltsova, Int. J. Hydrogen Energy, 31, 223 (2006).
[44]L. L. Jewell, B. H. Davis, Appl. Catal. A, 310, 1 (2006).
[45]W. Drexel, A. Murani, D. Tocchetti, W. Kley, I. Sosnowska, D. K. Ross, J. Phys. Chem. Solids, 37, 1135 (1976).
[46]Y. Z. Lu, C. Wang, W. J. Chen, J. Power Sources, 196, 3033 (2011).
[47]Y. Lu, Y. Jiang, H. Wu, W. Chen, J. Phys. Chem. C, 117, 2926 (2013).
[48]D. Hao, S. Xue-Zhao, S. Cheng-Min, H. Chao, X. Zhi-Chuan, L. Chen, T. Yuan, W. Deng-Ke, G. Hong-Jun, Chin. Phys. B, 19, 106104 (2010).
[49]M. Jin, H. Zhang, Z. Xieb, Y. Xia, Energy Environ. Sci., 5, 6532 (2012).